$[Cr(dpa)(ox)_2]^-$: a new bis-oxalato building block for the design of heteropolymetallic systems. Crystal structures and magnetic properties of $PPh_4[Cr(dpa)(ox)_2]$, $AsPh_4[Cr(dpa)(ox)_2]$, $Hdpa[Cr(dpa)(ox)_2]\cdot 4H_2O$, $Rad[Cr(dpa)(ox)_2]\cdot H_2O$ and $Sr[Cr(dpa)(ox)_2]_2\cdot 8H_2O$ (dpa = 2,2′-dipyridylamine)

Rodrigue Lescouëzec,[a] Gabriela Marinescu,[b] M. Carmen Muñoz,[c] Dominique Luneau,[d] Marius Andruh,[b] Francesc Lloret,[a] Juan Faus,[a] Miguel Julve,*[a] José Antonio Mata,[e] Rosa Llusar[f] and Joan Cano[g]

[a] *Departament de Química Inorgànica/Instituto de Ciencia Molecular, Facultat de Química de la Universitat de València, Dr. Moliner 50, 46100 Burjassot (València), Spain. E-mail: miguel.julve@uv.es*
[b] *Inorganic Chemistry Laboratory, Faculty of Chemistry, University of Bucharest, Str. Dumbrava Rosie nr. 23, 70254 Bucharest, Romania*
[c] *Departamento de Física Aplicada, Universidad Politécnica de València, Camino de Vera s/n, 46071 València, Spain*
[d] *Service de Chimie Inorganique et Biologique (CNRS UMR 5046), DMFMC, CEA-Grenoble, 17 rue des Martyrs, 38054 Grenoble cedex 09, France*
[e] *Departament de Química Inorgànica i Orgànica, Campus Riu Sec de la Universitat Jaume I, POB 224, 12080 Castelló, Spain*
[f] *Departament de Ciències Experimentals, Campus Riu Sec de la Universitat Jaume I, POB 224, 12080 Castelló, Spain*
[g] *Laboratoire de Chimie Inorganique (CNRS UMR 8613), Université de Paris-Sud, 91405 Orsay, France*

Received (in Strasbourg, France) 21st May 2001, Accepted 10th July 2001
First published as an Advance Article on the web 19th September 2001

The new complexes of formulae $PPh_4[Cr(dpa)(ox)_2]$ (**1**), $AsPh_4[Cr(dpa)(ox)_2]$ (**2**), $Hdpa[Cr(dpa)(ox)_2]\cdot 4H_2O$ (**3**), $Rad[Cr(dpa)(ox)_2]\cdot H_2O$ (**4**) and $Sr[Cr(dpa)(ox)_2]_2\cdot 8H_2O$ (**5**) [PPh_4 = tetraphenylphosphonium cation; $AsPh_4$ = tetraphenylarsonium cation; dpa = 2,2′-dipyridylamine; ox = oxalate dianion; Rad = 2-(4-*N*-methylpyridinium)-4,4,5,5-tetramethyl-4,5-dihydro-1*H*-imidazol-1-oxyl-3-*N*-oxide] have been prepared and characterised by single-crystal X-ray diffraction. The structures of **1–4** consist of discrete $[Cr(dpa)(ox)_2]^-$ anions, tetraphenylphosphonium (**1**), tetraphenylarsonium (**2**), monoprotonated Hdpa (**3**) and univalent radical (**4**) cations and uncoordinated water molecules (**2**–**4**). The chromium environment in **1**–**4** is distorted octahedral with Cr–O bond distances between 1.982(2)–1.946(2) Å and Cr–N bonds of 2.0716(17)–2.048(3) Å. The angles subtended at the chromium atom by the two oxalates are 83.6(2)–81.71(8)°, whereas the N–Cr–N angles are 87.76(7)–86.24(9)°. The $[Cr(dpa)(ox)_2]^-$ unit of **1**–**4** is also present in **5** but it acts as a chelating ligand through its two oxalato groups towards divalent strontium cations, yielding heterobimetallic zig-zag chains that run parallel to the *a* axis. Each chain is formed of diamond-shaped units sharing the strontium atoms, while the two other corners are occupied by two crystallographically independent chromium atoms. The $[Cr(dpa)(ox)_2]^-$ unit in **5** retains the environment observed in **1**–**4** and the strontium atom is coordinated to eight oxalate oxygens from four oxalate ligands. The two crystallographycally independent chromium centres within each double chain have opposite chirality. However, the adjacent double chains are related by an inversion centre resulting in achiral layers parallel to the *ac* plane. The magnetic properties of **1**–**5** have been investigated in the temperature range 1.9–290 K. A quasi Curie law behaviour is observed for **1**–**3** and **5** in agreement with their crystal structures, whereas a significant antiferromagnetic interaction between the chromium(III) and the radical centre occurs in the case of **4**. The synthetic possibilities offered by the use of the heteroleptic species $[CrL(ox)_2]^-$ (L = α-diimine-type ligand) as a ligand towards metal ions is analysed and discussed in the light of the available structural results.

The first studies of the coordinating ability of 2,2′-dipyridylamine (dpa) showed the great versatility of this ligand, which can act not only as a bidentate ligand through its two pyridyl nitrogen atoms[1–5] but also as a bridging ligand after removal of the amine hydrogen atom.[5,6] Interestingly, the free dpa ligand has a dimeric structure[7] in which two dpa molecules are linked by N–H···N hydrogen bonds, each dpa group exhibiting the *anti-syn* configuration [see Scheme 1(a)]. Most of the reported crystal structures of dpa-containing metal complexes concern the copper(II) ion with metal-to-dpa molar

 DOI: 10.1039/b104469a

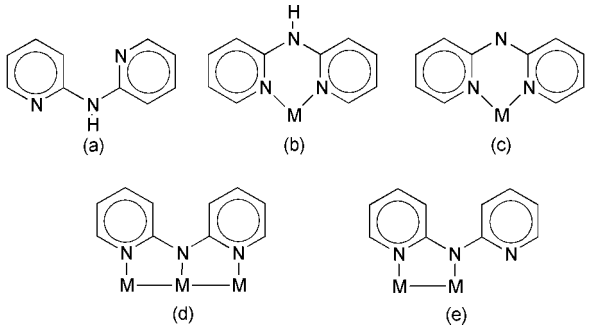

Scheme 1

ratios of 1 : 1 and 1 : 2,[8,9] the dpa ligand acting as a bidentate ligand through its two pyridyl nitrogen atoms [*anti-anti* conformation, Scheme 1(b)]. Although the resulting species are usually mononuclear, polynuclear complexes with a 1 : 1 Cu(II) : dpa molar ratio were obtained in the presence of suitable bridging ligands such as hydroxo,[8h] chloro,[8f] oxamidato[8c] and carbonato.[8d] Some years ago, copper(I) complexes with dpa were investigated as models for copper-containing plant hormone binding sites[10] and electrochemical studies showed that dpa favours the one-electron reduction from $[Cu(dpa)_2]^{2+}$ to $[Cu(dpa)_2]^{+}$ to a higher extent that the more rigid 2,2′-bipyridine (bpy) and 1,10-phenanthroline (phen).[11] Very recently, the unprecedented monodentate coordination mode of dpa through one of its two pyridyl atoms has been observed in the monuclear complex $[W(dpa)(CO)_5]$.[12] Finally, the uncommon monodeprotonated form of the dpa molecule can act also as a ligand towards first- and second-row transition metal ions, adopting either chelating [Scheme 1(c)][13] or bridging [Scheme 1(d,e)][14–19] coordination modes. Very interesting linear trinuclear complexes were reported in this latter case with the 2,2′-dipyridylamido exhibiting the *syn-syn* configuration.[15–19] Variable-temperature magnetic susceptibility studies on the trinuclear complexes revealed a remarkable diversity of magnetic behaviours ranging from strong antiferromagnetic coupling (tricopper and trinickel)[15,16] to spin crossover (tricobalt)[17a,c] and passing through Curie law behaviour (trichromium).[18]

In the context of our current research work devoted to the design of heterometallic complexes using as precursors heteroleptic chromium(III) mononuclear complexes that can be used as ligands,[20–22] we have synthesised a new family of compounds containing the bis(oxalato)(2,2′-dipyridylamine)chromium(III) unit. Their preparation, structural characterisation and magnetic properties are presented here.

Experimental

Materials

2,2′-Dipyridylamine, chromium(III) chloride hexahydrate, strontium(II) chloride hexahydrate, sodium oxalate, tetraphenylphosphonium chloride and tetraphenylarsonium chloride monohydrate were purchased from commercial sources and used as received. The radical salt 2-(4-*N*-methylpyridinium)-4,4,5,5-tetramethyl-4,5-dihydro-1*H*-imidazol-1-oxyl-3-*N*-oxide iodide was prepared as reported in the literature.[23] Elemental analyses (C, H, N) were carried out by the Microanalytical Service of the Universidad Autónoma de Madrid. The P : Cr (**1**), As : Cr (**2**) and Sr : Cr (**5**) molar ratios (1 : 1 for **1** and **2** and 0.5 : 1 for **5**) were determined by electron microscopy at the Servicio Interdepartamental de Investigación of the University of València.

Preparation of $XPh_4[Cr(dpa)(ox)_2]$, X = P (1) and As (2). An aqueous suspension (40 cm^3) containing chromium(III) chloride (2 mmol), dpa (2 mmol) and sodium oxalate (4 mmol) was refluxed under continuous stirring for 1.5 h. Tetraphenylphosphonium (**1**) or tetraphenylarsonium (**2**) chloride (2 mmol), dissolved in the minimum amount of warm water, was added to the previously filtered deep violet solution. A first crop of a pink (**1**) or violet (**2**) crystalline solid was obtained on standing. Single crystals as red prisms (**1**) or violet parallelepipeds (**2**) were grown from the mother liquor by slow evaporation at room temperature. Yield *ca.* 40% (**1** and **2**). Anal. calc. for $C_{38}H_{29}CrN_3O_8P$ (**1**): C, 61.81; H, 3.93; N, 5.69; found: C, 61.33; H, 3.86; N, 5.59%. Anal. calc. for $C_{38}H_{29}AsCrN_3O_8$ (**2**): C, 58.34; H, 3.71; N, 5.37; found: C, 58.01; H, 3.67; N, 5.29%.

Preparation of $Hdpa[Cr(dpa)(ox)_2]\cdot 4H_2O$ (3). The preparation of **3** is analogous to that of **1** and **2** except for the addition of a concentrated aqueous solution of HdpaCl (generated by reaction of stoichiometric amounts of dpa and dilute hydrochloric acid) to the filtered aqueous violet solution containing the $[Cr(dpa)(ox)_2]^-$ species. A first crop of a crystalline pink solid of **3** was formed on standing after half a day. Plate-like crystals of **3** suitable for X-ray diffraction separated from the mother liquor on slow evaporation at room temperature. Yield *ca.* 50%. The crystals of **3** lost water molecules after a few days. Anal. calc. for $C_{24}H_{27}CrN_6O_{12}$ (**3**): C, 44.81; H, 4.20; N, 13.06; found: C, 44.56; H, 4.13; N, 12.95%.

Preparation of $Rad[Cr(dpa)(ox)_2]\cdot H_2O$ (4). This complex was prepared as the previous one but the the radical cation as an iodide salt dissolved in the minimum amount of water (1 mmol, 10 cm^3) was added to the filtered violet aqueous solution containing the $[Cr(dpa)(ox)_2]^-$ complex (1 mmol, 25 cm^3). **4** separates as brown prismatic crystals from the mother liquor on slow evaporation at room temperature. Yield *ca.* 35%. Anal. calc. for $C_{27}H_{30}CrN_6O_{11}$ (**4**): C, 48.67; H, 4.50; N, 12.61; found: C, 48.54; H, 4.43; N, 12.52%.

Preparation of $Sr[Cr(dpa)(ox)_2]_2\cdot 8H_2O$ (5). The addition of complex **1** (0.25 mmol) to an aqueous solution of lithium perchlorate (0.25 mmol, 20 cm^3) under continuous stirring affords a violet solution containing the lithium salt of $[Cr(dpa)(ox)_2]^-$ and a white precipitate of PPh_4ClO_4. The white solid was removed by filtration and strontium chloride (0.125 mmol) dissolved in the minium amount of water added to the violet solution. Red prisms of **5** separated from this solution on slow evaporation at room temperature. The yield is practically quantitative. Anal. calc. for $C_{28}H_{34}Cr_2N_6O_{24}Sr$ (**5**): C, 32.64; H, 3.30; N, 8.15; found: C, 32.51; H, 3.23; N, 8.05%.

Physical techniques

IR spectra (4000–400 cm^{-1}) were recorded on a Bruker IF S55 spectrophotometer with samples prepared as KBr pellets. Variable temperature (1.9–290 K) magnetic susceptibilty measurements on polycrystalline samples were carried out with a Quantum Design SQUID operating at 0.5 T in the high temperature range (20–290 K) and at 250 G at $T < 20$ K in order to avoid saturation phenomena. Diamagnetic corrections for the constituent atoms were estimated from Pascal's constants[24] as -404×10^{-6} (**1**), -399×10^{-6} (**2**), -343×10^{-6} (**3**), -332×10^{-6} (**4**) and -248×10^{-6} (**5**) cm^3 mol^{-1} [per mol of Cr(III)].

Computational methodology

The computational strategy used in the present work here has been fully described elsewhere[25] and we will recall here only the relevant aspects. Density functional theory calculations[26] were done to evaluate the coupling constants concerning the the chromium(III)–radical and radical–radical pairs [see

Table 1 Crystallographic data for $PPh_4[Cr(dpa)(ox)_2]$ (**1**), $AsPh_4[Cr(dpa)(ox)_2]$ (**2**), $Hdpa[Cr(dpa)(ox)_2]\cdot 4H_2O$ (**3**), $Rad[Cr(dpa)(ox)_2]\cdot H_2O$ (**4**) and $Sr[Cr(dpa)(ox)_2]_2\cdot 8H_2O$ (**5**)

	1	**2**	**3**	**4**	**5**
Formula	$C_{38}H_{29}CrN_3O_8P$	$C_{38}H_{29}CrN_3O_8As$	$C_{24}H_{27}CrN_6O_{12}$	$C_{27}H_{30}CrN_6O_{11}$	$C_{28}H_{34}Cr_2N_6O_{24}Sr$
FW	738.61	782.56	643.52	666.57	1030.23
Crystal system	Monoclinic	Monoclinic	Triclinic	Monoclinic	Triclinic
Space group	$P2_1$	$P2_1$	$P\bar{1}$	$C2/c$	$P\bar{1}$
a/Å	9.2002(11)	9.2221(5)	9.294(2)	21.999(8)	9.457(2)
b/Å	13.4712(16)	13.471(3)	11.380(3)	16.248(4)	12.095(2)
c/Å	13.7964(16)	13.8725(17)	14.292(3)	17.111(4)	17.850(4)
α/°	90	90.0	93.78(2)	90	99.95(3)
β/°	97.574(3)	97.418(7)	95.838(14)	110.18(3)	99.57(3)
γ/°	90	90.0	111.39(2)	90	104.87(3)
U/Å^3	1695.0(3)	1709.0(4)	1391.6(5)	5741(3)	1895.5(7)
Z	2	2	2	8	2
T/K	293(2)	293(2)	293(2)	298(7)	293(2)
μ(Mo-Kα)/cm^{-1}	4.44	13.54	4.86	4.72	20.68
No. indep. refl.	13 778	2452	3611	6964	7110
No. obs. refl. $[I \geqslant 2\sigma(I)]$	9433	2050	3108	6964	4338
R_{int}	0.0203	0.0275	0.03680	0.0740	0.1006
R^a	0.0350	0.0340	0.0473	0.0654	0.0551
$R_w{}^b$	0.0531	0.0751	0.1249	0.1616	0.1405

^{a} $R = \Sigma(\|F_o| - |F_c\|)/\Sigma|F_o|$. ^{b} $R_w = [\Sigma_w(|F_o|^2 - |F_c|^2)^2]/[\Sigma_w|F_o|^2]^{1/2}$.

Scheme 2 and Fig. 9(a)] in **4**. Separate calculations were carried out for the high-spin (quartet and triplet spin states for the Cr(III)–rad and rad–rad pairs, respectively) and broken-symmetry low-spin states (triplet and singlet spin states for the Cr(III)–rad and rad–rad pairs, respectively). The hybrid B3LYP method[27] has been used in the calculations as implemented in GAUSSIAN 98,[28] mixing the exact Hartree–Fock exchange with Becke's expression for the exchange[29] and using the Lee–Yang–Parr correlation functional.[30] Basis sets of triple-ζ[31] with two extra p polarization functions (chromium atom) and of double-ζ quality[32] (atoms other than chromium) were used in our calculations.

The high spin–low spin energy gap (J) was evaluated from the calculated energies of the high spin (E_{hs}) and broken-symmetry low spin (E_{ls}) states through eqn. (1):

$$J = \frac{2(E_{ls} - E_{hs})}{S_{hs}(S_{hs} + 1) - S_{ls}(S_{ls} + 1)} \quad (1)$$

where S_{hs} and S_{ls} are the values of the total spin for the high- and low-spin states, respectively, dealing with the Cr(III)–rad and rad–rad pairs. The calculations were done on the real structures of the Cr–rad and rad–rad pairs as well as for the mononuclear paramagnetic units. Finally, spin density calculations were performed through Mulliken[33] and natural bond order (NBO)[34] analyses giving the same qualitative results.

Table 2 Selected bond lengths (Å) and angles (°)[a] for compounds **1** and **2**

	1	**2**
Cr–N(1)	2.0716(17)	2.092(7)
Cr–N(2)	2.0581(17)	2.054(6)
Cr–O(1)	1.9558(12)	1.944(4)
Cr–O(2)	1.9642(15)	1.948(5)
Cr–O(3)	1.9716(15)	1.977(5)
Cr–O(4)	1.9582(12)	1.966(5)
O(1)–Cr–O(2)	83.25(6)	83.6(2)
O(1)–Cr–O(4)	174.02(6)	174.4(2)
O(1)–Cr–N(1)	89.68(6)	89.0(2)
O(1)–Cr–N(2)	93.49(6)	93.9(2)
O(1)–Cr–O(3)	92.77(6)	92.5(2)
O(2)–Cr–O(4)	92.64(6)	93.1(2)
O(2)–Cr–N(1)	172.67(6)	172.3(2)
O(2)–Cr–N(2)	90.74(7)	91.2(2)
O(2)–Cr–O(3)	87.76(7)	88.1(2)
N(1)–Cr–O(4)	94.56(6)	94.5(2)
N(1)–Cr–N(2)	87.76(7)	87.6(3)
N(1)–Cr–O(3)	94.53(7)	93.9(3)
O(4)–Cr–N(2)	90.90(6)	90.7(2)
O(4)–Cr–O(3)	82.70(6)	82.9(2)
N(2)–Cr–O(3)	173.34(6)	173.5(2)

[a] Estimated standard deviations in the last significant digits are given in parentheses.

X-Ray data collection and structure refinement

Crystals were mounted on Bruker Smart CCD (**1** and **4**) and Enraf–Nonius CAD-4 (**2**, **3** and **5**) diffractometers and used for data collection. Diffraction data were collected at room temperature by using graphite-monochromated Mo-Kα radiation ($\lambda = 0.710\,73$ Å) with the $\omega - 2\theta$ method. Nominal crystal-to-detector distances of 4.0 and 5.9 cm were used for **1** and **4**, respectively. The unit cell parameters were determined from least-squares refinement on the setting angles from 25 centred reflections in the range $12 < \theta < 20°$ (**2**, **3** and **5**). In the case of **1** and **4**, the unit cell parameters were based upon least-squares refinement of three-dimensional centroids of 512 reflections. No significant fluctuations were observed in the intensities of three (**2**, **3** and **5**) standard reflections monitored periodically thoughout data collection. An hemisphere of data for **1** was collected based on one ω-scan run (starting $\omega = 28°$) at $\phi = 0$ with the detector at $2\theta = 28°$. For this run, a total of 606 frames were collected at 0.3° intervals and 30 s per frame. A total of 1271 (**1**) and 1321 (**4**) frames of data were collected using a narrow-frame method with scan widths of 0.3° in ω and exposure times of 30 (**1**) and 10 s (**4**) per frame. Intensity data for **1**–**5** were corrected for Lorentz and polarisation effects and absorption corrections made. The diffraction frames of **1** and **4** were integrated using the SAINT package[35] and corrected for absorption with SADABS.[36] A summary of the crystallographic data and structure refinement is given in Table 1.

The structures of **1**–**5** were solved by direct methods and refined by the full-matrix least-squares method on F^2. The computations were performed with the SHELXTL 5.10

package[37] (**1** and **4**) and SHELX 86 and SHELXL 97 programs[38] (**2**, **3** and **5**). All non-hydrogen atoms were refined anisotropically. The amine hydrogen atom of dpa in **1**–**4** and the proton of $Hdpa^+$ in **3** were found in difference maps and refined isotropically. The remaining hydrogen atoms of **1**–**5** were set in calculated positions and refined isotropically with a common fixed isotropic thermal parameter. Concerning complex **1**, the crystal was modeled as a racemic twin with a Flack parameter of 0.13 improving the residual parameters. The final full-matrix least-squares refinement on F^2, minimizing the function $\Sigma w[(|F_o|)^2 - (|F_c|)^2]^2$ with $w = 1/[\sigma^2(F_o^2) + (mP)^2 + nP]$ and $P = (F_o^2 + 2F_c^2)/3$ [$m = 0.0331$ (**1**), 0.0457 (**2**), 0.1105 (**3**), 0.1098 (**4**) and 0.0869 (**5**); $n = 0$ (**1**), 1.0914 (**2**), 2.0131 (**3**), 0.0 (**4**) and 1.7274 (**5**), converged at the values of R and R_w listed in Table 1. The values of f, f' and f'' were taken from ref. 39. The molecular plots were drawn with the ORTEP program.[40] Selected bond lengths and angles are gathered in Tables 2 (**1** and **2**), 3 (**3**), 4 (**4**) and 5 (**5**).

CCDC reference numbers 161709–161713. See http://www.rsc.org/suppdata/nj/b1/b104469a/ for crystallographic data in CIF or other electronic format.

Results and discussion

IR characterisation

The most relevant features of the IR spectrum of free dpa are the sharp peaks at 3250m (N–H stretching), 1605s and 1566m (N–H deformation and C=N and C=C stretchings) and 768s and 735m cm^{-1} (C–H out-of-plane deformation). The shift towards higher wavenumbers of the N–H stretching of dpa in the IR spectra of **1**–**5** [medium and broad absorption at 3435 (**1**), 3445 (**2**), 3440 (**3**), 3455 (**4**) and 3420 (**5**) cm^{-1}] indicates that it is coordinated.[3] The broadening observed in all these high frequency features suggests the presence of hydrogen bonds in **1**–**5**,[41] as confirmed by X-ray diffraction. The out-of-plane bending vibrations of the phenyl rings of the tetraphenylphosphonium (**1**) and tetraphenylarsonium (**2**) cations occur at 690, 722 and 762 cm^{-1} for the former and at 693, 740 and 753 cm^{-1} for the latter. The occurrence of a medium absorption at 1656 cm^{-1} in the IR spectrum of **3**, which is assigned to the N–H deformation of the protonated amine of dpa, is in agreement with the presence of $Hdpa^+$ in this complex. In this respect, it deserves to be pointed out that this peak is located at 1654 cm^{-1} in the IR spectrum of $HdpaClO_4$. The peaks of the the nitronyl nitroxide radical in the IR spectra of **4** (main peaks at 1638, 1563, 1421, 1380, 1322, 1172 and 833 cm^{-1}) are in the same positions as those observed in the spectra of its iodide salt, suggesting that the radical is uncoordinated in **4**. Finally, as far as the oxalato peaks are concerned, slight but significant differences are observed between the IR spectra of **5** and those of **1**–**4**: three peaks at 1709s, 1680s and 1654s cm^{-1} (**5**) and at 1716s, 1700s and 1680s cm^{-1} (**1**–**4**) [ν_{as}(CO)]; two peaks at 1409s and 1264 cm^{-1} (**5**) and at 1360s and 1240m (**1** and **2**), 1380s and 1245m (**3**) and 1370s and 1235m cm^{-1} (**4**) [ν_s(CO)]; a sharp medium intensity peak at 810 (**5**), and at 805 (**1** and **2**) and 800 cm^{-1} (**3** and **4**) [δ(OCO)]. The different coordination mode of oxalato in **5** *vs.* that in **1**–**4** (see structural discussion) would account for these spectral differences.

Description of the X-ray structures

$PPh_4[Cr(dpa)(ox)_2]$ (1) and $AsPh_4[Cr(dpa)(ox)_2]$ (2). The crystal structures of the isostructural complexes **1** and **2** are made up of discrete tris-chelated $[Cr(phen)(ox)_2]^-$ anions and either PPh_4^+ (**1**) (Fig. 1) or $AsPh_4^+$ (**2**) cations (Fig. 2) that are held together by electrostatic forces and Van der Waals interactions. Interestingly, the tris-chelated anions are linked through hydrogen bonds between the amine hydrogen [H(3)] and one oxalate oxygen [O(8a)] atom [N(3)···O(8a) = 2.97(10) (**1**) and 2.98(10) Å (**2**) and N(3)–H(3)···O(8a) = 152.0(1) (**1**) and 138.6(1)° (**2**); a = 1 + *x*, *y*, *z*], leading to a chain of chromium atoms that runs parallel to the *x* axis (Fig. 3).

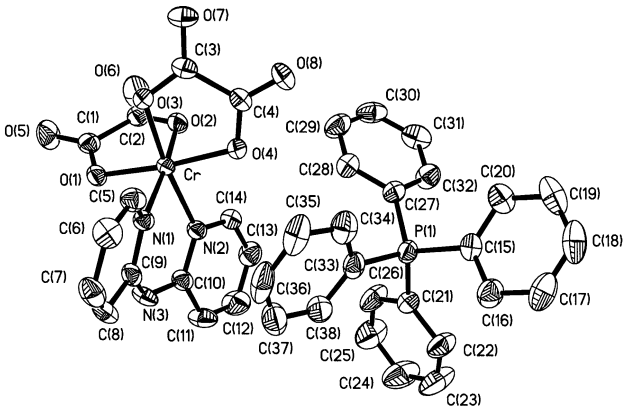

Fig. 1 Perspective view of compound **1** along with the atom numbering. The thermal ellipsoids are drawn at the 50% probability level and the hydrogen atoms have been omitted for clarity.

Each chromium atom in **1** and **2** is coordinated by two dpa nitrogen and four oxalate oxygen atoms, taking on a distorted octahedral geometry. The narrow bites of the bidentate dpa [87.76(7) (**1**) and 87.6(3)° (**2**) for N(1)–Cr–N(2)] and ox ligands [83.25(6) (**1**) and 83.6(2)° (**2**) for O(1)–Cr–O(2), 82.70(6) (**1**) and 82.9(2)° (**2**) for O(4)–Cr–O(3)] are the main factors accounting for the distortion of the metal environment from the ideal octahedron. The four Cr–O(ox) bond distances are very close [values varying in the ranges 1.9558(17)–1.9716(15) (**1**) and 1.944(4)–1.977(5) Å (**2**)] and they compare well with the average value reported in the parent heteroleptic $[Cr(phen)(ox)_2]^-$ [1.948(2)–1.962(4) Å],[22,42] $[Cr(bpm)(ox)_2]^-$ [1.945(6) Å],[21] $[Cr(hm)(ox)_2]^-$ [1.974(2) Å][43] and $[Cr(bpy)(ox)_2]^-$ [1.953(2) Å][20c] mononuclear species (phen = 1,10-phenanthroline, bpm = 2,2′-bipyrimidine, hm = histamine and bpy = 2,2′-bipyridine). The Cr–N(dpa) bond distances [2.0716(17) and 2.0581(17) Å (**1**); 2.092(7) and 2.054(6) Å (**2**)] are somewhat longer than the Cr–O(ox) ones. The two ox ligands do not exhibit significant deviations from planarity and they form dihedral angles of 68.85(6) (**1**) and 68.86(18)° (**2**). The carbon–carbon bond distance in the ox ligands is as expected for a single C–C bond [C(1)–C(2) = 1.566(3) (**1**) and 1.533(11) Å (**2**); C(3)–C(4) = 1.550(3) (**1**)

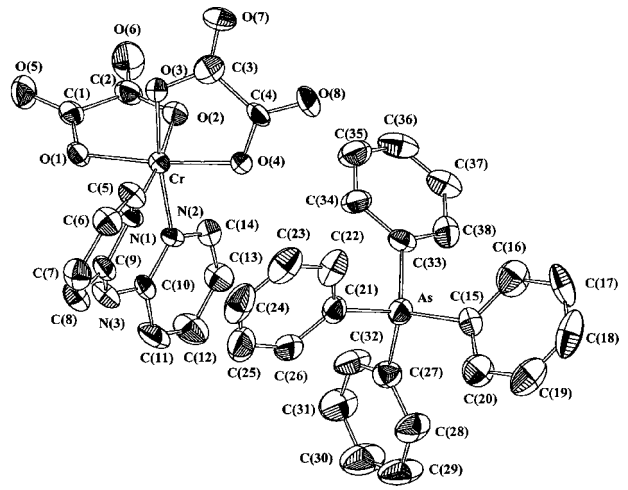

Fig. 2 Perspective view of compound **2** along with the atom numbering. The thermal ellipsoids are drawn at the 30% probability level and the hydrogen atoms have been omitted for clarity.

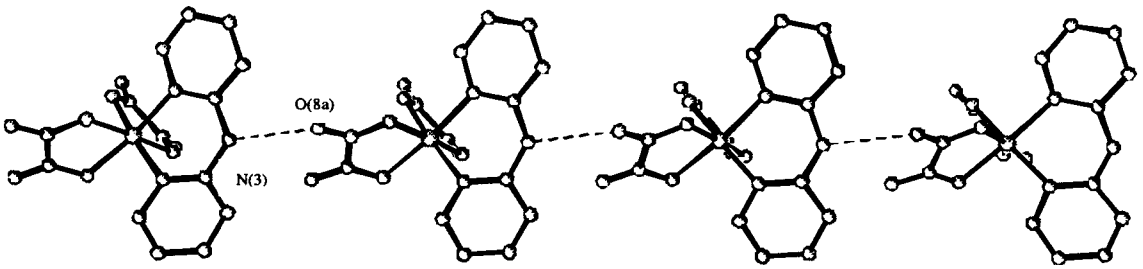

Fig. 3 A view along the *x* axis of the chain arrangement of the $[Cr(dpa)(ox)_2]^-$ units in **1** connected by hydrogen bonds.

and 1.546(11) Å (**2**)]. The average values for the peripheral and inner C–O bonds are 1.216(3) (**1**) [1.216(10) (**2**)] and 1.289(2) (**1**) [1.298(9) Å (**2**)], respectively, the greater double bond character of the free C–O bonds accounting for the shorter values. The dpa molecule acts as a bidentate ligand towards the chromium atom through its two pyridine nitrogen atoms, N(1) and N(2). The six-membered Cr–N(1)–C(9)–N(3)–C(10)–N(2) chelate ring adopts the boat conformation with the Cr and N(3) atoms 0.56 (**1**) [0.227(3) (**2**)] and 0.23 (**1**) [0.237(5) Å (**2**)], respectively, below the plane defined by the remaining four atoms. The individual pyridine rings in the dpa ligand are essentially planar [maximum deviation 0.021 Å at C(9) in **1** and **2**], but the ligand itself is not, with a 26.1(1) (**1**) [25.3(3)° (**2**)] dihedral angle between the planes defined by the pyridine rings. This value is very close to that of the free dpa (23°)[7] and this twist serves to relieve the steric hindrance within the ligand. The bond distances and angles about chemically equivalent atoms in the two pyridine rings are practically identical and there is no distortion about the bridging nitrogen [N(3)–C(9) = 1.374(3) (**1**) and 1.372(10) Å (**2**); N(3)–C(10) = 1.375(3) (**1**) and 1.380(10) Å (**2**)]. The average values of the intra-ring C–C and C–N bond distances are 1.376(4) (**1**) [1.372(12) (**2**)] and 1.347(3) (**1**) [1.343(10) Å (2)], respectively. The bulky XPh_4^+ cations [X = P (**1**) and As (**2**)] exhibit the expected tetrahedral shape with average X–C bond distances of 1.797(3) (**1**) and 1.919(8) Å (**2**), and average C–X–C angles of 109.5(1) (**1**) and 109.5(4)° (**2**).

Interestingly, edge-to-face phenyl–phenyl interactions[44] between the XPh_4^+ cations occur along the *y* axis (see Fig. 4), the X···X(b) (b = $-x$, $y + 0.5$, $1 - z$) distances involved being 6.807(1) (**1**) and 6.8(1) Å (**2**). No significant graphite-like interactions are observed between the pyridine rings of adjacent $[Cr(dpa)(ox)_2]^-$ units. The chromium–chromium separation within the hydrogen bonded chain [Cr···Cr(a) = 9.20(1) (**1**) and 9.11(8) Å (**2**)] is much longer than the shortest chromium–chromium separation [Cr···Cr(b) = 7.43(1) (**1**) and 7.43(9) Å (**2**)]. The shortest Cr···X distances are 6.467(1) (**1**) and 6.506(1) Å (**2**).

Hdpa[Cr(dpa)(ox)$_2$]·4H$_2$O (3). The structure of complex **3** consists of discrete $[Cr(dpa)(ox)_2]^-$ anions, monoprotonated $Hdpa^+$ cations (see Fig. 5) and crystallisation water molecules, which are held together by electrostatic forces, Van der Waals interactions and an extensive network of hydrogen bonds involving the water molecules, four oxalate oxygen atoms [O(3), O(5), O(6) and O(8)] and the $Hdpa^+$ cation (see end of Table 3). The hydrogen bonds within the $[Cr(dpa)(ox)_2]^-/Hdpa^+$ ion pair are shown in Fig. 6.

As in **1** and **2**, the environment of the chromium atom is distorted octahedral, the largest deviations from the ideal octahedron being caused by the narrow bites of the bidentate dpa [86.53(11)°] and ox ligands [81.95(10) and 82.26(9)° for O(1)–Cr–O(2) and O(3)–Cr–O(4), respectively]. The four Cr–O(ox) bond distances vary in the range 1.962(2)–1.982(2) Å and they are somewhat shorter than the Cr–N(dpa) ones [2.048(3) and 2.067(3) Å]. The two ox ligands are planar and they form a dihedral angle of 74.72(9)°. The carbon–carbon bond distances [1.553(5) and 1.527(5) Å for C(11)–C(12) and C(13)–C(14), respectively] and the average values for the per-

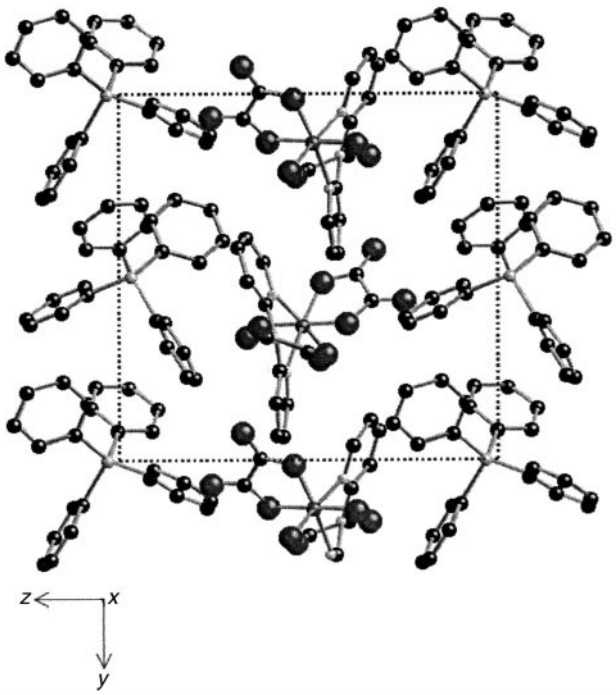

Fig. 4 A projection of the crystal packing of **2** through the *x* axis.

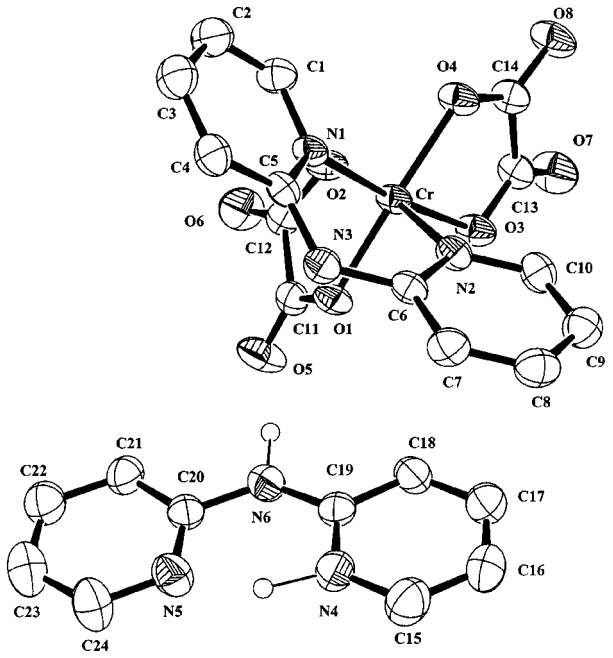

Fig. 5 Perspective view of the $Hpda^+$ and $[Cr(dpa)(ox)_2]^-$ ions of compound **3** with the atom numbering. The thermal ellipsoids are drawn at the 30% probability level. The hydrogen atoms and the water molecules have been omitted for clarity.

Table 3 Selected bond lengths (Å) and angles (°)[a] for compound **3**

Chromium environment			
Cr–N(1)	2.048(3)	Cr–N(2)	2.067(3)
Cr–O(1)	1.968(2)	Cr–O(2)	1.971(2)
Cr–O(3)	1.982(2)	Cr–O(4)	1.962(2)
N(1)–Cr–N(2)	86.53(11)	N(1)–Cr–O(2)	90.42(10)
N(1)–Cr–O(3)	173.29(9)	N(1)–Cr–O(1)	94.53(10)
N(1)–Cr–O(4)	91.13(10)	N(2)–Cr–O(3)	95.25(10)
N(2)–Cr–O(2)	170.02(10)	N(2)–Cr–O(1)	88.81(10)
N(2)–Cr–O(4)	96.08(10)	O(2)–Cr–O(3)	88.86(10)
O(2)–Cr–O(1)	81.95(10)	O(2)–Cr–O(4)	93.48(10)
O(3)–Cr–O(1)	91.97(9)	O(3)–Cr–O(4)	82.26(9)
O(1)–Cr–O(4)	172.74(9)		
dpa ligand			
N(1)–C(1)	1.365(4)	N(1)–C(5)	1.341(4)
C(1)–C(2)	1.358(5)	C(2)–C(3)	1.395(5)
C(3)–C(4)	1.354(5)	C(4)–C(5)	1.400(5)
N(3)–C(5)	1.385(4)	N(3)–C(6)	1.390(4)
N(2)–C(6)	1.356(4)	N(2)–C(10)	1.360(4)
C(6)–C(7)	1.392(5)	C(7)–C(8)	1.372(5)
C(8)–C(9)	1.387(5)	C(9)–C(10)	1.369(5)
N(1)–C(1)–C(2)	122.8(3)	C(1)–C(2)–C(3)	118.6(3)
C(2)–C(3)–C(4)	119.4(3)	C(3)–C(4)–C(5)	119.9(3)
C(4)–C(5)–N(1)	120.9(3)	C(5)–N(1)–C(1)	118.3(3)
C(4)–C(5)–N(3)	119.6(3)	N(1)–C(5)–N(3)	119.5(3)
C(5)–N(3)–C(6)	127.4(3)	N(3)–C(6)–N(2)	120.6(3)
N(3)–C(6)–C(7)	117.9(3)	C(6)–C(7)–C(8)	120.1(3)
C(7)–C(8)–C(9)	118.9(3)	C(8)–C(9)–C(10)	118.6(3)
C(9)–C(10)–N(2)	123.6(3)	C(10)–N(2)–C(6)	117.2(3)
N(2)–C(6)–C(7)	121.4(3)		
$Hpda^+$ cation			
N(4)–C(15)	1.359(59)	N(4)–C(19)	1.340(5)
C(15)–C(16)	1.346(6)	C(16)–C(17)	1.400(6)
C(17)–C(18)	1.367(6)	C(18)–C(19)	1.397(5)
N(6)–C(19)	1.357(5)	N(6)–C(20)	1.407(5)
N(5)–C(20)	1.320(5)	N(5)–C(24)	1.336(5)
C(20)–C(21)	1.392(5)	C(21)–C(22)	1.382(6)
C(22)–C(23)	1.380(6)	C(23)–C(24)	1.364(6)
N(4)–C(15)–C(16)	120.5(4)	C(15)–C(16)–C(17)	118.7(4)
C(16)–C(17)–C(18)	120.4(4)	C(17)–C(18)–C(19)	119.3(4)
C(18)–C(19)–N(4)	118.7(3)	C(19)–N(4)–C(15)	122.3(3)
C(18)–C(19)–N(6)	121.9(3)	N(4)–C(19)–N(6)	119.3(3)
C(19)–N(6)–C(20)	129.5(3)	N(6)–C(20)–N(5)	117.2(3)
N(6)–C(20)–C(21)	119.2(3)	C(20)–C(21)–C(22)	118.0(4)
C(21)–C(22)–C(23)	118.7(4)	C(22)–C(23)–C(24)	118.8(4)
C(23)–C(24)–N(5)	123.8(4)	C(24)–N(5)–C(20)	117.1(4)
N(5)–C(20)–C(21)	123.6(3)		
Hydrogen bonds[b]			
D	A	D···A	∠D–H···A
N(4)	N(5)	2.642(4)	150(5)
N(6)	O(5)	2.900(4)	170(5)
O(10)	O(5)	2.85(2)	
O(11)	O(3)	2.82(2)	
O(12)	O(6)	2.89(2)	
O(12)	O(8)	2.84(2)	
O(9)	O(10)	2.76(2)	
O(9)	O(11)	2.78(2)	
O(9)	O(12)	2.80(2)	
O(10)	O(11)	2.73(2)	

[a] Estimated standard deviations in the last significant digits are given in parentheses. [b] D = donor; A = acceptor.

ipheral [1.221(4) Å] and inner C–O [1.293(4) Å] bonds of the oxalate ligands are in agreement with those observed in **1** and **2**. The dpa molecule acts as a bidentate ligand towards the chromium atom through its two pyridine nitrogen atoms, N(1) and N(2) thus exhibiting the *anti-anti* conformation. The resulting six-membered Cr–N(1)–C(5)–N(3)–C(6)–N(2) chelate ring adopts the boat conformation with the Cr and N(3) atoms 0.298(1) and 0.304(2) Å, respectively, below the plane defined by the remaining four atoms. The individual pyridine rings in the dpa ligand are planar [maximum deviation 0.012(3) Å at C(3)]. However, they form a dihedral angle of 32.57(15)°, a value that is somewhat greater than those observed for the dpa ligand in **1** and **2**. The occurrence of the monoprotonated $Hdpa^+$ species as a counterion in **3** allows the comparison of its structure and that of coordinated dpa in the same system for the first time (see Table 3). Previous structural reports on the complexes $[Cu(dpa)_2(NCO)](SO_4)_{1/2}\cdot dpa\cdot H_2O$[9f] and $[Mo_2(CF_3CO_2)_4(CF_3CO_2H)_2]\cdot 2dpa$[14] revealed the coexistence of both coordinated and free dpa molecules in the same compound, the

Table 4 Selected bond lengths (Å) and angles (°)[a] for compound **4**

Chromium environment			
Cr–N(1)	2.049(2)	Cr–N(2)	2.070(2)
Cr–O(1)	1.946(2)	Cr–O(3)	1.958(2)
Cr–O(5)	1.977(2)	Cr–O(7)	1.9677(19)
N(1)–Cr–N(2)	86.24(9)	N(1)–Cr–O(3)	90.62(9)
N(1)–Cr–O(5)	175.94(9)	N(1)–Cr–O(1)	92.48(9)
N(1)–Cr–O(7)	94.23(9)	N(2)–Cr–O(5)	93.97(9)
N(2)–Cr–O(3)	173.28(9)	N(2)–Cr–O(1)	90.73(9)
N(2)–Cr–O(7)	94.23(9)	O(3)–Cr–O(5)	89.59(9)
O(3)–Cr–O(1)	83.47(9)	O(3)–Cr–O(7)	91.93(9)
O(5)–Cr–O(1)	91.58(9)	O(5)–Cr–O(7)	81.71(8)
O(1)–Cr–O(7)	171.90(8)		
Radical cation			
O(11)–N(11)	1.272(2)	O(12)–N(12)	1.264(4)
N(11)–C(21)	1.353(4)	N(12)–C(21)	1.355(4)
N(11)–C(22)	1.498(4)	N(12)–C(25)	1.496(4)
C(22)–C(23)	1.516(5)	C(25)–C(26)	1.513(5)
C(22)–C(24)	1.526(5)	C(25)–C(27)	1.517(5)
C(22)–C(25)	1.557(4)	C(21)–C(28)	1.454(4)
C(28)–C(29)	1.395(4)	C(28)–C(33)	1.401(4)
C(29)–C(30)	1.366(5)	C(32)–C(33)	1.358(5)
N(13)–C(30)	1.344(4)	N(13)–C(32)	1.346(4)
N(13)–C(31)	1.476(4)		
O(11)–N(11)–C(21)	126.8(3)	O(12)–N(12)–C(21)	126.2(3)
O(11)–N(11)–C(22)	120.0(2)	O(12)–N(12)–C(25)	121.0(3)
C(21)–N(11)–C(22)	112.7(2)	C(21)–N(12)–C(25)	112.7(3)
N(11)–C(22)–C(25)	101.1(2)	N(12)–C(25)–C(22)	101.1(2)
N(11)–C(22)–C(23)	109.5(3)	N(12)–C(25)–C(26)	106.4(3)
N(11)–C(22)–C(24)	106.4(3)	N(12)–C(25)–C(27)	109.3(3)
C(23)–C(22)–C(25)	115.7(3)	C(26)–C(25)–C(22)	114.1(3)
C(23)–C(22)–C(24)	109.0(3)	C(26)–C(25)–C(27)	110.4(3)
N(11)–C(21)–C(28)	126.0(3)	N(12)–C(21)–C(28)	126.0(3)
N(11)–C(21)–N(12)	108.1(3)	C(21)–C(28)–C(29)	121.6(3)
C(21)–C(28)–C(33)	121.7(3)	C(29)–C(28)–C(33)	116.7(3)
C(28)–C(33)–C(32)	120.4(3)	C(28)–C(29)–C(30)	120.5(3)
C(33)–C(32)–N(13)	121.6(3)	C(29)–C(30)–N(13)	121.3(3)
C(32)–N(13)–C(31)	119.8(3)	C(30)–N(13)–C(31)	120.7(3)
C(30)–N(13)–C(32)	119.5(3)		

[a] Estimated standard deviations in the last significant digits are given in parentheses.

free dpa adopting the *anti-syn* and *anti-anti* conformation modes, respectively. The presence of the proton H(4) bound to N(4) [1.17(6) Å for H(4)–N(4)] and its hydrogen bond with N(5) accounts for the *anti-anti* conformation of $Hdpa^+$ and the quasi coplanarity of its two pyridine rings [the dihedral angle between the N(4)–C(15)–C(16)–C(17)–C(18)–C(19) and N(5)–C(20)–C(21)–C(22)–C(23)–C(24) mean planes is only 3.21(12)°]. Bond distances and angles about chemically equivalent atoms in dpa are practically identical whereas significant differences are observed within $Hpda^+$, which are attributed to the asymmetry of the N(4)–H(4)···N(5) intramolecular hydrogen bond: 1.320(5) [N(5)–C(20)] *vs.* 1.340(5) Å [N(4)–C(19)] and 1.336(5) [N(5)–C(24)] *vs.* 1.359(5) Å [N(4)–C(15)], for instance. Partial π–π overlap between pyridine rings of pairs of $Hdpa^+$ cations [3.82(4) Å] and $[Cr(dpa)(ox)_2]^-$ anions [4.00(2) Å] along the *x* axis are observed (see Fig. 7). The shortest chromium-chromium separation is 6.32(4) Å [Cr···Cr(a) with a = $-x$, $-y$, $1-z$].

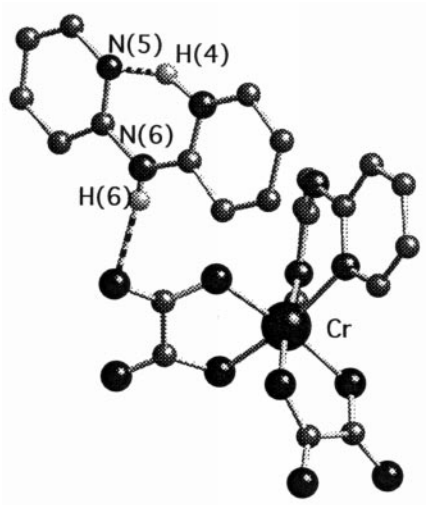

Fig. 6 A view of the hydrogen bonding between $Hdpa^+$ and $[Cr(dpa)(ox)_2]^-$ ions in **3**.

Rad[Cr(dpa)(ox)$_2$]·H$_2$O (4). The structure of **4** consists of $[Cr(dpa)(ox)_2]^-$ anions, *p-N*-methylpyridinium nitronyl nitroxide radicals (Rad^+) and a water molecule of crystallisation (see Fig. 8). Hydrogen bonds involving the uncoordinated water molecule (O), the amine nitrogen atom of dpa [N(3)] and three oxalate oxygens [O(4), O(6) and O(7)] [2.855(4), 2.893(4) and 2.899(5) Å for O···O(4a), N(3)···O(6b) and O···O(7), respectively with 167(4), 175(4) and 172(3)° for O–H(20)···O(7), O–H(10)···O(4a) and N(3)–H(3N)···O(6b); symmetry codes: a = $3/2-x$, $1/2-y$, $2-z$ and b = x, $1-y$, $1/2+z$] provide additional stability to the lattice.

The chromium environment is distorted octahedral as in **1**–**3**, the main distortion being caused by the short bite of the bidentate dpa [86.24(9)° for N(1)–Cr–N(2)] and ox ligands [83.47(9) and 81.71(8)° for O(3)–Cr–O(1) and O(5)–Cr–O(7), respectively]. The pyridyl rings of dpa are planar [largest deviations are 0.17 Å at C(3) for one ring and 0.28 Å at C(9) for the second ring] but the ligand as a whole is not [the

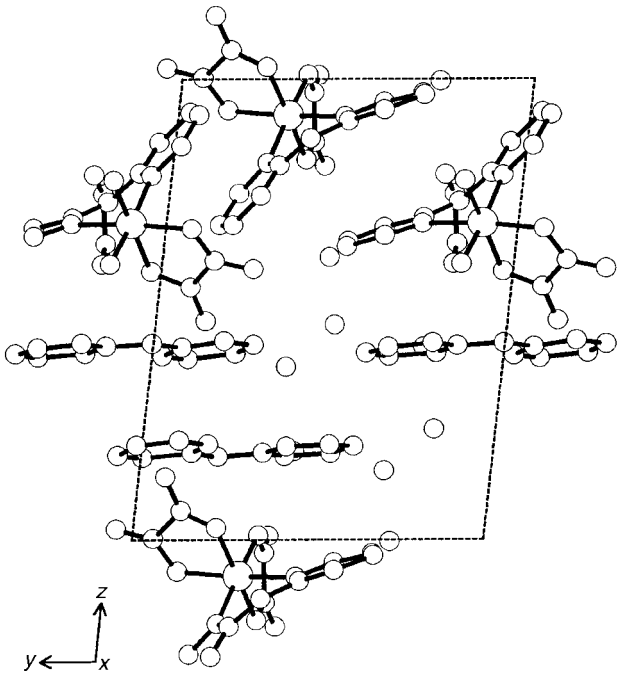

Fig. 7 A projection of the crystal packing of **3** through the *x* axis.

dihedral angle between the two pyridyl rings is 26.98°]. As in **1**–**3**, the six-membered Cr–N(1)–C(5)–N(3)–C(6)–N(2) chelate ring adopts the boat conformation with the Cr and N(3) atoms being 0.764 and 0.218 Å, respectively, below the plane defined by the remaing four atoms. The two ox ligands are not strictly planar and the oxygen atoms are slightly twisted around the C–C bond so that the carbon atoms for both ox ligands are in the mean plane of the six atoms but the oxygen atoms are ±0.60 Å away in one ox ligand and ±0.50 Å away in the second one. This results in dihedral angles between the two O–C–O planes of 5.22° at one ox ligand and 6.60° at the other one. The dihedral angle between the mean planes of the two ox ligands is 76.07°. The carbon–carbon bond distances [1.533(4) and 1.540(4) Å for C(11)–C(12) and C(13)–C(14), respectively] and the main values for the peripheral [1.215(4) Å] and inner C–O [1.297(4) Å] bonds of the ox ligands are comparable with those observed in **1**–**3**.

The bond distances and angles found for the radical cation agree with previous findings for *N*-alkylpyridinium nitronyl nitroxide radicals.[23,45,46] The pyridyl ring is planar and it makes a dihedral angle of 8.96° with the mean plane of the

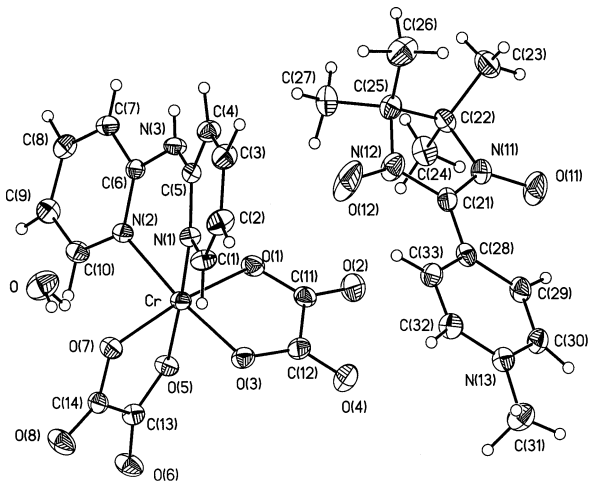

Fig. 8 Perspective view of compound **4** along with the atom numbering. The thermal ellipsoids are drawn at the 30% probability level.

O(11)–N(11)–C(21)–N(12)–O(12) π system containing the unpaired electron. This is a rather small value compared with those generally reported in substituted nitronyl nitroxides.[23,45–49] The shortest distance between the two radical cations is 3.750(7) Å for O(11)···N(11c) (symmetry code c = 1 − *x*, *y*, 1/2 − *z*). The dihedral angle between the two NO groups is 34.7°. From previous theoretical work, it is known that short contacts between two NO groups may lead to noticeable magnetic interactions.[47] Their magnitude and sign rely both on the separation and the relative orientation of the π* orbitals that contain the unpaired electrons. In compound **4**, the distance between the two NO groups and their relative orientation are far from the optimum 3 Å in a head-to-tail arrangement. This is assumed not to favour a strong overlap, and hence only a weak antiferromagnetic interaction is expected to occur between the radicals. In addition, the shortest distance between the radical cation and the chromium complex involves one of the NO groups [N(12)–O(12)] and the O(2) oxalato oxygen atom [3.410(4) Å for N(12)···O(2)]. These two contacts lead to a discrete Cr_2Rad_2 unit, which is depicted in Scheme 2. The overall distance separating the NO group from the Cr(III) is 4.65(1) Å and the shortest metal–metal separation is 6.793(1) Å. A very weak π–π interaction between the pyridyl rings of dpa ligands of adjacent $[Cr(dpa)(ox)_2]^-$ units is also observed, the significant slipping of the rings leading to a very slight overlap. Finally, there is a very weak overlap between the pyridine rings of two adjacent radicals, the separation between the two centres of the pyridyl rings being 4.29 Å. Given that the spin density on the pyridine rings is extremely weak, the magnetic interactions through this pathway is neglected.

$Sr[Cr(dpa)(ox)_2]_2 \cdot 8H_2O$ (5). The structure of compound **5** is made up of crystallographically independent heterotrinuclear species of formula $\{Sr[Cr(dpa)(ox)_2]_2\}$ (Fig. 9) that grow along the *x* axis through oxalato bridges, yielding neutral double zigzag chains (Fig. 10). Each chain is formed of diamond shaped units sharing the strontium atoms, while the other two corners are occupied by chromium atoms having opposite chirality. Adjacent double chains are related by an inversion centre leading to an achiral arrangement in the *xz* plane (Fig. 10). An extensive network of hydrogen bonds (see end of Table 5) involving all the water molecules, the dpa amine nitrogen atoms and nine of the sixteen oxalate oxygens contributes to the stabilisation of the structure. The interchain π–π interactions are very weak, the shortest separation between pyridyl rings of dpa ligands being *ca.* 4 Å.

The two crystallographically independent chromium atoms [Cr(1) and Cr(2)] are six-fold coordinated with two nitrogen atoms from a bidentate dpa ligand and four oxygen atoms from two bis-bidentate oxalate groups building a distorted octahedron around each metal atom. The Cr–N bond lengths [mean value 2.05 Å] are somewhat longer than the Cr–O ones

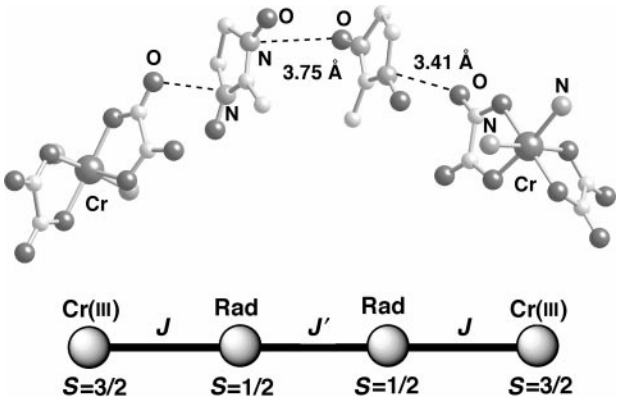

Scheme 2 Exchange coupling patterns within the Cr_2Rad_2 unit.

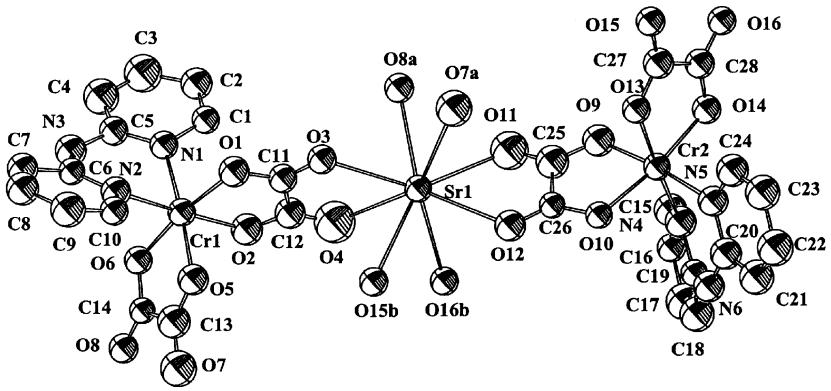

Fig. 9 Perspective drawings of the crystallographically independent unit of compound **5** with the atom numbering. The thermal ellipsoids are drawn at the 30% probability level. The hydrogen atoms and water molecules have been omitted for clarity.

[average value 1.97 Å]. The angles subtended at the chromium atom by the dpa [values of 86.4(13) to 87.5(4)°] and ox [values varying in the range 82.3(3)–82.8(3)°] ligands are in agreement with those observed in the previous structures. The dpa ligands exhibit the *anti-anti* conformation and they are bound to the chromium atoms through the pyridine nitrogen atoms. The pyridyl rings of the dpa ligands are planar as expected but the entire dpa ligands deviate significantly from planarity [37.2(6) and 21.2(6)° for the dpa ligands at Cr(1) and Cr(2), respectively]. The six-membered chelate rings made by the bidentate dpa groups at each chromium atom adopt the boat conformation with significant deviation of the chromium atoms [0.295(5) and 0.270(5) Å for Cr(1) and Cr(2), respectively] and the corresponding amine nitrogens {0.261(8) [N(3)] and 0.242(8) Å [N(6)]} from the plane defined by the remaining four dpa atoms. The oxalato ligands are planar and they form dihedral angles of 78.9(3) [Cr(1)] and 80.6(3)° [Cr(2)].

The strontium atom is eight-fold coordinated by eight oxygens of four bis-bidentate oxalate ligands. The Sr–O bond distances vary in the range 2.607(10)–2.729(10) Å, values which are in agreement with those observed in reported structures with divalent strontium.[50] The O–Sr–O bite angles of the bis-bidentate oxalato ligands are very acute [values varying in the range 61.8(3)–63.1(3)°]. The carbon–carbon bond lengths of the oxalate ligands agree with those observed in **1**–**4** [C–C bond distance varying between 1.543(16) and 1.559(18) Å]. The C–O bonds within each oxalato are significantly different {the shortest and longest values being 1.206(14) Å [C(12)–O(4)] and 1.279(14) Å [C(25)–O(9)]} as expected due to the different nature and charge of the cations they bridge.

The intrachain metal–metal separations are 5.925(3) [Cr(1)···Sr(1)], 5.962(3) [Cr(2)···Sr(1)], 7.245(4) [Cr(1)···Cr(2)] and 9.457(2) Å [Sr(1)···Sr(1a); a = 1 + *x*, *y*, *z*]. The shortest homo- and heterometallic interchain metal–metal distances are 6.731(5) [Cr(1)···Cr(1b); b = −*x*, −*y*, 1 − *z*], 6.445(6) [Cr(2)···Cr(2c); c = 1 − *x*, −*y*, −*z*] and 10.291(5) Å [Sr(1)···Sr(1d); d = 1 − *x*, 1 − *y*, 1 − *z*].

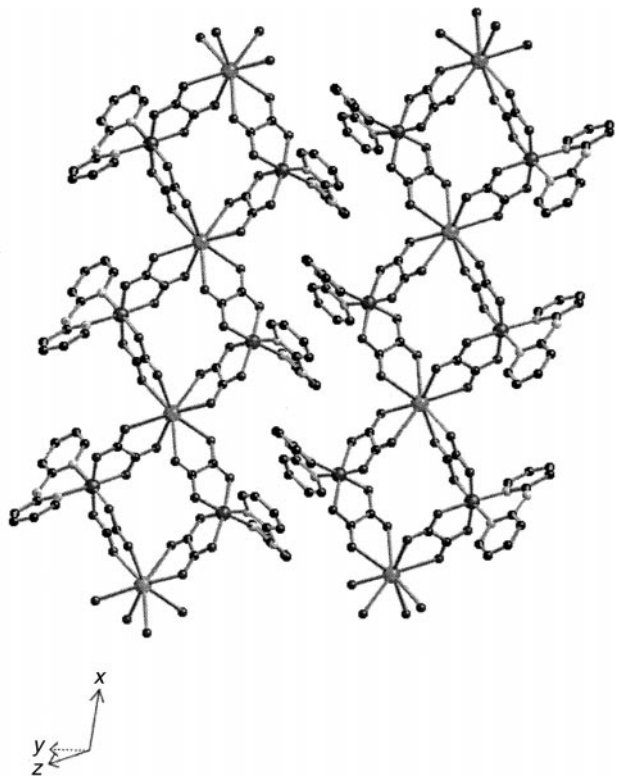

Fig. 10 View of the double chain arrangement of **5** in the *xz* plane.

Magnetic properties of 1–5

The temperature dependence of $\chi_M T$ for **1**–**5** [χ_M being the magnetic susceptibility per mol of chromium(III)] in the temperature range 1.9–100 K is shown in Fig. 11. At 290 K, the values of $\chi_M T$ are 1.87 (**1**–**3** and **5**) and 2.24 (**4**) cm^3 K mol^{-1}. These values are as expected for a magnetically isolated spin quartet ($S_{Cr} = 3/2$; **1**–**3** and **5**) and for a pair of non-interacting quartet ($S_{Cr} = 3/2$) and doublet ($S_{rad} = 1/2$) spin states (**4**). The value of $\chi_M T$ for **1**–**3** and **5** remains practically constant down to 30 K and it exhibits a small decrease at lower temperatures to reach 1.63 (**1**), 1.74 (**2**), 1.61 (**3**) and 1.80

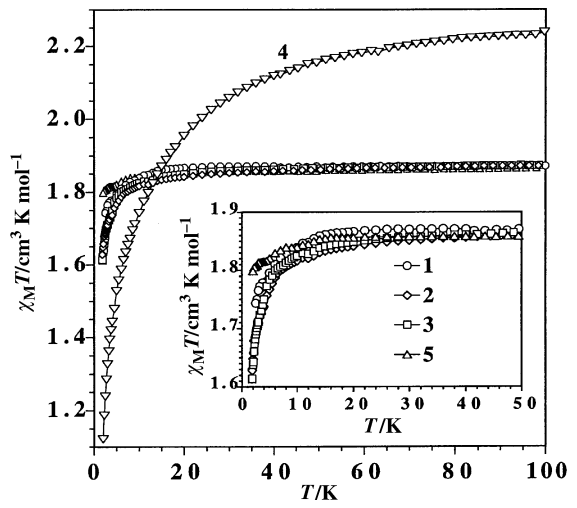

Fig. 11 $\chi_M T$ *vs.* *T* plots for complexes **1**–**5**. The solid line for **4** corresponds to the best fit using eqn. (2) (see text). The inset shows the the low temperature region in detail.

Table 5 Selected bond lengths (Å) and angles (°)[a] for compound **5**

Chromium environment			
Cr(1)–N(1)	2.063(9)	Cr(2)–N(4)	2.035(9)
Cr(1)–N(2)	2.044(9)	Cr(2)–N(5)	2.058(10)
Cr(1)–O(1)	1.978(8)	Cr(2)–O(9)	1.974(8)
Cr(1)–O(2)	1.987(8)	Cr(2)–O(10)	1.969(7)
Cr(1)–O(5)	1.968(8)	Cr(2)–O(13)	1.971(8)
Cr(1)–O(6)	1.954(7)	Cr(2)–O(14)	1.976(8)
N(1)–Cr(1)–N(2)	86.4(4)	N(4)–Cr(2)–N(5)	87.5(4)
N(1)–Cr(1)–O(2)	92.9(4)	N(2)–Cr(2)–O(14)	93.5(4)
N(1)–Cr(1)–O(5)	175.1(3)	N(4)–Cr(2)–O(10)	92.4(4)
N(1)–Cr(1)–O(1)	92.7(4)	N(4)–Cr(2)–O(9)	90.6(4)
N(1)–Cr(1)–O(6)	92.5(3)	N(4)–Cr(2)–O(13)	175.9(4)
N(2)–Cr(1)–O(5)	92.4(4)	N(5)–Cr(2)–O(10)	91.9(3)
N(2)–Cr(1)–O(2)	177.7(4)	N(5)–Cr(2)–O(14)	94.4(4)
N(2)–Cr(1)–O(1)	95.6(4)	N(5)–Cr(2)–O(9)	174.1(4)
N(2)–Cr(1)–O(6)	91.7(3)	N(5)–Cr(2)–O(13)	94.0(4)
O(2)–Cr(1)–O(5)	88.5(4)	O(10)–Cr(2)–O(14)	171.5(3)
O(2)–Cr(1)–O(1)	82.3(3)	O(10)–Cr(2)–O(9)	82.6(3)
O(2)–Cr(1)–O(6)	90.6(3)	O(10)–Cr(2)–O(13)	91.4(3)
O(5)–Cr(1)–O(1)	92.1(4)	O(14)–Cr(2)–O(9)	91.3(4)
O(5)–Cr(1)–O(6)	82.8(3)	O(14)–Cr(2)–O(13)	82.6(3)
O(1)–Cr(1)–O(6)	171.3(3)	O(9)–Cr(2)–O(13)	88.2(4)
Strontium environment			
Sr(1)–O(3)	2.607(10)	Sr(1)–O(11)	2.658(10)
Sr(1)–O(4)	2.729(10)	Sr(1)–O(12)	2.671(9)
Sr(1)–O(7a)	2.631(10)	Sr(1)–O(15b)	2.705(9)
Sr(1)–O(8a)	2.638(8)	Sr(1)–O(16b)	2.659(9)
O(3)–Sr(1)–O(7a)	87.4(3)	O(8a)–Sr(1)–O(11)	72.9(3)
O(3)–Sr(1)–O(8a)	70.0(3)	O(8a)–Sr(1)–O(12)	126.5(3)
O(3)–Sr(1)–O(16b)	125.7(3)	O(8a)–Sr(1)–O(15b)	145.3(3)
O(3)–Sr(1)–O(11)	142.4(3)	O(8a)–Sr(1)–O(4)	87.9(3)
O(3)–Sr(1)–O(12)	141.9(3)	O(16b)–Sr(1)–O(11)	85.2(3)
O(3)–Sr(1)–o(15b)	76.6(3)	O(16b)–Sr(1)–O(12)	70.7(3)
O(3)–Sr(1)–O(4)	61.8(3)	O(16b)–Sr(1)–O(15b)	61.8(3)
O(7a)–Sr(1)–O(8a)	63.1(3)	O(16b)–Sr(1)–O(4)	70.8(3)
O(7a)–Sr(1)–O(16b)	144.7(3)	O(11)–Sr(1)–O(12)	62.4(3)
O(7a)–Sr(1)–O(11)	70.9(3)	O(11)–Sr(1)–O(15b)	141.0(3)
O(7a)–Sr(1)–O(12)	75.3(3)	O(11)–Sr(1)–O(4)	122.6(3)
O(7a)–Sr(1)–O(15b)	125.1(3)	O(12)–Sr(1)–O(15b)	86.0(3)
O(7a)–Sr(1)–O(4)	144.2(3)	O(12)–Sr(1)–O(4)	140.4(3)
O(8a)–Sr(1)–O(16b)	134.4(3)	O(15b)–Sr(1)–O(4)	67.9(3)
Possible hydrogen bonds			
N(3)···O(17c)	2.86(2)	O(9)···O(20)	2.853(14)
N(6)···O(18)	2.82(2)	O(11)···O(23)	3.04(2)
O(3)···O(17)	2.786(19)	O(11)···O(24)	2.86(2)
O(3)···O(22)	2.860(18)	O(15)···O(19b)	2.92(2)
O(4)···O(24)	2.94(2)	O(15)···O(22d)	2.99(2)
O(4)···O(20b)	2.94(2)	O(16)···O(18)	2.735(13)
O(5)···O(19)	2.900(13)	O(16)···O(24d)	2.98(2)
O(7)···O(22b)	2.91(2)	O(18)···O(23b)	2.94(2)
O(8)···O(21)	2.853(16)		

[a] Estimated standard deviations in the last significant digits are given in parentheses. [b] Symmetry codes: a = $x + 1$, y, z; b = $x - 1$, y, z; c = x, $2 - y$, $1 - z$; d = $x - 2$, y, z.

(**5**) cm^3 K mol^{-1} at 1.9 K. Zero-field splitting effects (D) and/or very weak magnetic interactions between the local spin quartets would account for the small decrease in $\chi_M T$ of **1**–**3** and **5** in the low temperature region. This is not surprising in the light of their structures [mononuclear Cr(III) units in **1**–**3** and oxalato-bridged bimetallic Cr(III)–Sr(II) chains in **5**]. It can also be concluded that the efficiency of the N–H···O(ox) hydrogen bonding pattern of **1** and **2** in mediating magnetic interactions between the Cr(III) ions is extremely low, if any.

Interestingly, $\chi_M T$ for **4** exhibits a significant decrease at $T < 100$ K and it reaches a value of 1.25 cm^3 K mol^{-1} at 1.9 K. Such a value is clearly below those of complexes **1**–**3** and **5**, indicating that significant antiferromagnetic interactions occur between the spins of the chromium and radical cations. Taking into account the Cr(1)–rad(1)–rad(2)–Cr(2) tetrameric entity present in **4** (Scheme 2), we have analysed its magnetic data through the isotropic Hamiltonian of eqn. (2):

$$\hat{H} = -J[\hat{S}_{Cr1} \cdot \hat{S}_{rad1} + \hat{S}_{Cr2} \cdot \hat{S}_{rad2}] - J'[\hat{S}_{rad1} \cdot \hat{S}_{rad2}] + g_{Cr1} H\beta \hat{S}_{Cr1} + g_{Cr2} H\beta \hat{S}_{Cr2} + g_{rad1} H\beta \hat{S}_{rad1} + g_{rad2} H\beta \hat{S}_{rad2} + D_{Cr}[\hat{S}_z{}^2 - 1/3S(S+1)] \quad (2)$$

where J and J' refer to the exchange coupling parameters within the Cr–rad and rad–rad pairs, $g_{Cr1} = g_{Cr2}$ and $g_{rad1} = g_{rad2}$ are the Landé factors for the Cr(III) and radical centres, while the last term accounts for an axial zero-field splitting for the Cr(III) ion with $S = 3/2$. No theoretical analytical expression is known for this Hamiltonian and the theoretical analysis of the magnetic data of **4** has been performed by means of the VPMAG program.[51] The energy matrix is built for this tetrameric entity considering all the microstates for two close and very small values of the external magnetic field

(H). This allows us to calculate the magnetic susceptibility at zero field as $\chi_M = \delta M/\delta H$ where M is the magnetisation. The best agreement between the experimental and calculated susceptibility data is obtained for $J = -3.1$ cm^{-1}, $J' = -12.5$ cm^{-1}, $g_{Cr} = 1.97$ and $g_{rad} = 2.01$, $|D| = 0.91$ cm^{-1} with $R = 3.1 \times 10^{-5}$ {R is the agreement factor defined as $\Sigma_i[(\chi_M T)_{obs}(i) - (\chi_M T)_{calc}(i)]^2/\Sigma_i[(\chi_M T)_{obs}(i)]^2$}. The computed values of the g factors and D are physically reasonable and the calculated curve (solid line in Fig. 11) matches the magnetic data very well.

The values of the antiferromagnetic interactions for both the Cr(III)–rad and rad–rad pairs in **4** are small but significant. In order to substantiate both the nature and magnitude of these magnetic interactions, we have carried out density functional theory (DFT) calculations on the real structures of the rad–rad and Cr(III)–rad pairs present in **4** (Scheme 2) and also on the isolated radical and mononuclear chromium(III) complex. The calculated values of J (-5 cm^{-1}) and J' (-18.2 cm^{-1}) agree both in sign and magnitude with those obtained from the fit. Spin density calculations on the $[Cr(dpa)(ox)_2]^-$ [Scheme 3(a)] and Rad^+ [Scheme 3(b)] units allowed us to understand the nature of the magnetic interactions through the intermolecular contacts in **4**. In the case of the radical [Scheme 3(b)], a positive spin density of *ca.* one-half electron is distributed on each NO unit and a negative spin density of *ca.* 1/5 electron is located on the carbon atom that is bound to both NO fragments. The negative spin density on this carbon atom, as well as the others that appear in the system, are due to the spin polarization mechanism. In such a mechanism, one atom having a spin density tends to induce a spin density of the opposite sign on the neighbouring atoms. The same mechanism is operative through space (intermolecular interactions) and thus, the NO group of one radical unit in **4** polarizes the spin density of the NO group of the neighbouring unit, which is in a quasi-eclipsed conformation (see Scheme 2) and the antiferromagnetic coupling results in the rad–rad pair. An analogous situation occurs in the Cr–rad pair. The three unpaired electrons of the Cr(III) ion in octahedral geometry are of the t_{2g} type and one of them, denoted d_{xz} (Scheme 4), delocalises some positive spin density on the $2p_z$ orbitals of the oxalate oxygens. Looking at the Cr–rad pair (Scheme 2), one can see how the polarisation of the spin density of the neighbouring NO group by that of the $2p_z$ orbital of the oxalate oxygen through the π pathway is symmetry-adapted and it accounts for the weak but significant antiferromagnetic coupling observed in the Cr–rad pair.

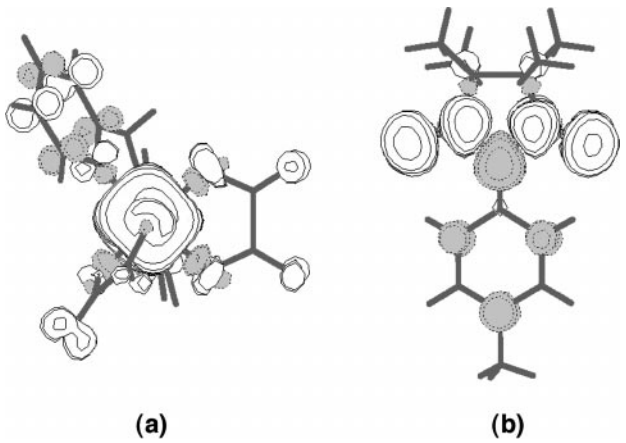

Scheme 3 Spin density maps of the Cr (a) and Rad (b) units. Opposite signs of spin density values are denoted by the white and shaded areas.

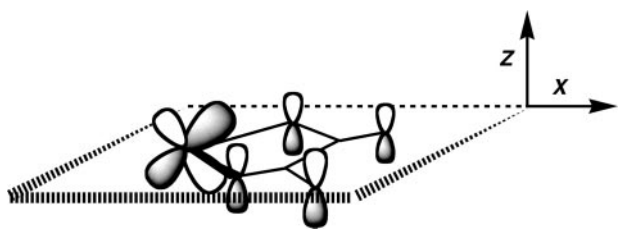

Scheme 4

In summary, the new building block of formula $[Cr(dpa)(ox)_2]^-$ has been prepared and structurally characterised with the diamagnetic XPh_4^+ [X = P (**1**) and As (**2**)] and the unprecedented monoprotonated $Hdpa^+$ (**3**) species as counterions. The use of a radical cation as counterion (complex **4**) allowed us to observe significant antiferromagnetic interactions through space in the Cr(III)–rad and rad–rad pairs. Finally, the structure of the bimetallic double zig-zag chain occurring in **5** shows the potential versatility of the $[Cr(dpa)(ox)_2]^-$ unit to generate interesting self-assembling frameworks with divalent cations, which could exhibit interesting magneto-optical properties. Further work using this building block with paramagnetic metal ions is currently under way.

Acknowledgements

Financial support from the Spanish Dirección General de Investigación Científica y Técnica (DGICYT) through Projects PB97-1397 and PB98-1044, the Romanian Ministry of Education (Grants 30C/CNCSIS and 1D/CNCSIS) and the TMR Program from the European Union (Contract ERBFMRXCT98-0181) is acknowledged. Thanks are also extended to the Centre d'Informàtica de la Universitat de València for computer resource support.

References

1 A. W. Meibohm, S. Bellman and L. Leth, *Proc. Indiana Acad. Sci.*, 1956, **66**, 95.
2 S. Kirschner, *Inorg. Synth.*, 1957, **5**, 14.
3 (*a*) W. R. McWhinnie, *J. Chem. Soc.*, 1964, 5165; (*b*) W. R. McWhinnie, *Coord. Chem. Rev.*, 1970, **5**, 293.
4 J. Goodgame, *J. Chem. Soc. A*, 1966, 63.
5 T. J. Hurley and M. A. Robinson, *Inorg. Chem.*, 1968, **7**, 33.
6 J. F. Geldard and F. Lyons, *J. Am. Chem. Soc.*, 1962, **84**, 2262.
7 J. E. Johnson and R. A. Jacobson, *Acta Crystallogr., Sect. B*, 1973, **29**, 1669.
8 (*a*) R. A. Jacobson and W. P. Jensen, *Inorg. Chim. Acta*, 1981, **52**, 205; (*b*) N. Ray, S. Tyagi and B. Hathaway, *Acta Crystallogr., Sect. B*, 1982, **38**, 1574; (*c*) J. Sletten, *Acta Chem. Scand. Ser. A*, 1982, **36**, 345; (*d*) J. Sletten, *Acta Chem. Scand. A*, 1984, **38**, 491; (*e*) S. Aduldecha and B. J. Hathaway, *Acta Crystallogr., Sect. C*, 1991, **47**, 84; (*f*) I. I. Mathews and H. Manohar, *Acta Crystallogr., Sect. C*, 1991, **47**, 1621; (*g*) P. Akhter, P. Fitzsimmons and B. Hathaway, *Acta Crystallogr., Sect. C*, 1991, **47**, 308; (*h*) L. P. Wu, M. E. Keniry and B. Hathaway, *Acta Crystallogr., Sect. C*, 1992, **48**, 35; (*i*) S. Youngme, C. Pakawatchai and H. K. Fun, *Acta Crystallogr., Sect. C*, 1998, **54**, 451; (*j*) S. Youngme, C. Pakawatchi, H. K. Fun and K. Chinnakali, *Acta Crystallogr., Sect. C*, 1998, **54**, 1586.
9 (*a*) J. E. Johnson, T. A. Beineke and R. A. Jacobson, *J. Chem. Soc. A*, 1971, 1371; (*b*) J. E. Johnson and R. A. Jacobson, *J. Chem. Soc., Dalton Trans.*, 1973, 580; (*c*) W. P. Jensen and R. A. Jacobson, *Inorg. Chim. Acta*, 1981, **49**, 199; (*d*) A. Walsh, B. Walsh, B. Murphy and B. J. Hathaway, *Acta Crystallogr., Sect. B*, 1981, **37**, 1512; (*e*) R. A. Jacobson and W. P. Jensen, *Inorg. Chim. Acta*, 1986, **114**, L9; (*f*) P. Akhter and B. Hathaway, *Acta Crystallogr., Sect. C*, 1991, **47**, 86; (*g*) S. Aduldecha, M. E. Keniry, P. Akhter, S. Tyagi and B. J. Hathaway, *Acta Crystallogr., Sect. C*, 1991, **47**, 1378; (*h*) M. C. Muñoz, J. M. Lázaro, J. Faus and M. Julve, *Acta Crystallogr., Sect. C*, 1993, **49**, 1756; (*i*) S. Youngme, K. Chandavong, C. Pakawatchai, Z. Y. Zhou and H. K. Fun, *Acta Crystallogr., Sect. C*, 1998, **54**, 199; (*j*) S. Youngme, K. Poopasit, H. K. Fun, K. Chinnakali, I. A. Razak and S. Chantrapromma, *Acta Crystallogr., Sect. C*, 1998, **54**, 1221; (*k*) S. Youngme, K. Poopasit, K. Chinnakali, I. A. Chatrapromma and H. K. Fun, *Inorg. Chim. Acta*, 1999, **292**, 57; (*l*) J. L. Mesa, K. Urtiaga, L. Lezama and M. I. Arriortua, *Acta Chem. Scand.*, 1999, **53**, 634; (*m*) S. Youngme, C. Pakawatchai, W. Somjitsripunya, K. Chinnakali and H. K. Fun, *Inorg. Chim. Acta*, 2000, **303**, 181.

10 (*a*) J. S. Thompson and J. F. Whitney, *Inorg. Chem.*, 1984, **23**, 2813; (*b*) G. Pyrka, R. J. Seeney and A. A. Pinkerton, *Acta Crystallogr., Sect. C*, 1991, **47**, 510.
11 A. Cinquantini, G. Opromolla and P. Zanello, *J. Chem. Soc., Dalton Trans.*, 1991, 3161.
12 B. S. Creaven, R. A. Howie and C. Long, *Acta Crystallogr., Sect. C*, 2000, **56**, e181.
13 O. R. Rodig, T. Brueckner, B. K. Hurlburt, R. K. Schlatzer, T. L. Venable and E. Sinn, *J. Chem. Soc., Dalton Trans.*, 1981, 196.
14 M. C. Suen, Y. Y. Wu, J. D. Chen, T. C. Keng and J. C. Wang, *Inorg. Chim. Acta*, 1999, **288**, 82.
15 L. P. Wu, P. Field, T. Morrissey, C. Murphy, P. Nagle, B. Hathaway, C. Simmons and P. Thornton, *J. Chem. Soc., Dalton Trans.*, 1990, 3835.
16 (*a*) S. Aduldecha and B. Hathaway, *J. Chem. Soc., Dalton Trans.*, 1991, 993; (*b*) R. Clérac, F. A. Cotton, K. R. Dunbar, C. A. Murillo, I. Pascual and X. Wang, *Inorg. Chem.*, 1999, **38**, 2655.
17 (*a*) E. C. Yang, M. C. Cheng, M. S. Tsai and S. M. Peng, *J. Chem. Soc., Chem. Commun.*, 1994, 2377; (*b*) F. A. Cotton, L. M. Daniels, G. T. Jordan, IV and C. Murillo, *J. Am. Chem. Soc.*, 1977, **119**, 10377; (*c*) R. Clérac, F. A. Cotton, K. R. Dunbar, T. Lu, C. A. Murillo and X. Wang, *Inorg. Chem.*, 2000, **39**, 3065.
18 (*a*) R. Clérac, F. A. Cotton, L. M. Daniels, K. R. Dunbar, C. A. Murillo and I. Pascual, *Inorg. Chem.*, 2000, **39**, 748; (*b*) R. Clérac, F. A. Cotton, L. M. Daniels, K. R. Dunbar, C. A. Murillo and I. Pascual, *Inorg. Chem.*, 2000, **39**, 752.
19 J. T. Sheu, C. C. Lin, I. Chao, C. C. Wang and S. M. Peng, *Chem. Commun.*, 1996, 315.
20 (*a*) F. D. Rochon, R. Melanson and M. Andruh, *Inorg. Chem.*, 1996, **35**, 6086; (*b*) M. Andruh, R. Melanson, C. V. Stager and F. Rochon, *Inorg. Chim. Acta*, 1996, **251**, 309; (*c*) M. C. Muñoz, M. Julve, F. Lloret, J. Faus and M. Andruh, *J. Chem. Soc., Dalton Trans.*, 1998, 3125.
21 G. de Munno, D. Armentano, M. Julve, F. Lloret, R. Lescouëzec and J. Faus, *Inorg. Chem.*, 1999, **38**, 2234.
22 G. Marinescu, M. Andruh, R. Lescouëzec, M. C. Muñoz, J. Cano, F. Lloret and M. Julve, *New J. Chem.*, 2000, **24**, 527.
23 K. Awaga, T. Inabe, U. Nagashima, T. Kakamura, M. Matsumoto, Y. Kawabata and Y. Maruyama, *Chem. Lett.*, 1991, 1777.
24 A. Earshaw, *Introduction to Magnetochemistry*, Academic Press, London, 1968.
25 E. Ruiz, P. Alemany, S. Alvarez and J. Cano, *J. Am. Chem. Soc.*, 1997, **119**, 1297.
26 R. G. Parr and W. Yang, *Density Functional Theory of Atoms and Molecules*, Oxford University Press, New York, 1989.
27 A. D. Becke, *J. Chem. Phys.*, 1993, **98**, 5648.
28 M. J. Frisch, G. W. Trucks, H. B. Schlegel, G. E. Scuseria, M. A. Robb, J. R. Cheeseman, V. G. Zakrzewski, J. A. Montgomery, R. E. Stratmann, J. C. Burant, S. Dapprich, J. M. Millam, A. D. Daniels, K. N. Kudin, M. C. Starin, O. Farkas, J. Tomasi, V. Barone, M. Cossi, R. Cammi, B. Mennucci, C. Pomelli, C. Adamo, S. Clifford, J. Ochterski, G. A. Petersson, P. Y. Ayala, Q. Cui, K. Morokuma, D. K. Malick, A. D. Rabuck, K. Raghavachari, J. B. Foresman, J. Cioslowski, J. V. Ortiz, B. B. Stefanov, G. Liu, A. Liashenko, P. Piskorz, I. Komaromi, R. Gomperts, R. L. Martin, D. J. Fox, T. Keith, M. A. Al-Laham, C. Y. Peng, A. Nanayakkara, C. Gonzalez, M. Challacombe, P. M. W. Gill, B. G. Johnson, W. Chen, M. W. Wong, J. L. Andres, M. Head-Gordon, E. S. Replogle and J. A. Pople, GAUSSIAN 98, Rev. A.7, Gaussian Inc., Pittsburg, PA, 1998.
29 A. D. Becke, *Phys. Rev. A*, 1988, **38**, 3098.
30 C. Lee, W. Yang and R. G. Parr, *Phys. Rev. B*, 1988, **37**, 785.
31 A. Schaefer, C. Huber and R. Ahlrichs, *J. Chem. Phys.*, 1994, **100**, 5829.
32 A. Schaefer, H. Horn and R. Ahlrichs, *J. Chem. Phys.*, 1992, **97**, 2571.
33 R. S. Mulliken, *J. Chem. Phys.*, 1962, **36**, 3428.
34 (*a*) J. E. Carpenter and F. Weinhold, *THEOCHEM*, 1988, **169**, 41; (*b*) A. E. Reed, L. A. Curtiss and F. Weinhold, *Chem. Rev.*, 1988, **88**, 899.
35 SAINT, v. 5.0, Bruker Analytical X-ray Systems, Madison, WI, 1998.
36 G. M. Sheldrick, SADABS, Empirical Absorption Program, University of Göttingen, Germany, 1996.
37 *SHELXTL*, v. 5.1, Bruker Analytical X-ray Systems, Madison, WI, 1997.
38 (*a*) G. M. Sheldrick, SHELXL 97, Program for Crystal Structure Determination, University of Göttingen, Germany, 1986; (*b*) G. M. Sheldrick, SHELX 93, Program for the Refinement of Crystal Structures, University of Göttingen, Germany, 1997.
39 *International Tables for X-ray Crystallography*, Kynoch Press, Birmingham, 1974, vol. 4, p. 99.
40 C. K. Jonhson, ORTEP, Report ORNL-3794; Oak Ridge National Laboratory, Oak Ridge, TN, 1971.
41 K. Nakamoto, *Infrared and Raman Spectra of Inorganic and Coordination Compounds*, Wiley, New York, 4th edn., 1986, p. 228.
42 F. D. Rochon and G. Massarweh, *Can. J. Chem.*, 1999, **77**, 2059.
43 N. Sakagami, E. Kita, P. Kita, J. Wísniewska and S. Kaizaki, *Polyhedron*, 1999, **18**, 2001.
44 (*a*) I. Dance and M. Scudder, *J. Chem. Soc., Chem. Commun.*, 1995, 1039; (*b*) I. Dance and M. Scudder, *Chem. Eur. J.*, 1996, **2**, 481.
45 K. Awaga and N. Wada, in *Magnetism: A Supramolecular Function*, NATO ASI Ser., Ser. C, ed. O. Kahn, Kluwer, Dordrecht, 1996, vol. 484, pp. 205–218.
46 G. Ballester, E. Coronado, C. Giménez-Saiz and F. M. Romero, *Angew. Chem., Int. Ed.*, 2000, **40**, 792.
47 A. Caneschi, D. Gatteschi and P. Rey, *Prog. Inorg. Chem.*, 1991, **39**, 331.
48 A. Cogne, J. Laugier, D. Luneau and P. Rey, *Inorg. Chem.*, 2000, **39**, 5510.
49 M. Deumal, J. Cirujeda, J. Veciana and J. J. Novoa, *Chem. Eur. J.*, 1999, **5**, 1631.
50 (*a*) C. Robl and A. Weiss, *Z. Naturforsch. B: Anorg. Chem. Org. Chem. B*, 1986, **41**, 1490; (*b*) C. Robl, V. Gnutzmann and A. Weiss, *Z. Anorg. Allg. Chem.*, 1987, **549**, 187.
51 J. Cano, VPMAG, University of València, Spain, 2001.